Influence of the Fluid-to-Film Transition on Photophysical Properties of MLCT Excited States in a Polymerizable Dimethacrylate Fluid

Troy E. Knight, Anna P. Goldstein, M. Kyle Brennaman, Thomas Cardolaccia, Ashish Pandya, Joseph M. DeSimone, and Thomas J. Meyer*

Department of Chemistry, The University of North Carolina, Chapel Hill, North Carolina 27599, United States

Received: July 29, 2010; Revised Manuscript Received: October 12, 2010

Photophysical properties of the salts $[Ru(bpy)_3](p\text{-}Tos)_2$, $[Ru(dmb)_3](PF_6)_2$, $[Ru(vbpy)_3](PF_6)_2$, and $[Ru(phen)_3](p\text{-}Tos)_2$ (bpy = 2,2′-bipyridine, dmb = 4,4′-dimethyl-2,2′-bipyridine, vbpy = 4-methyl-4′-vinyl-2,2′-bipyridine, phen = 1,10-phenanthroline, and *p*-Tos = *p*-toluene sulfonate) in fluid and film polyethylene glycol dimethacrylate containing nine ethylene glycol spacers (PEG-DMA550) are reported. MLCT absorption energies and bandshapes are similar in fluid and film PEG-DMA550 pointing to similar local dielectric environments, presumably dominated by the polar acrylate groups. Emission energies and excited-to-ground state 0−0 energy gaps (E_0), determined by emission spectral fitting, are blue-shifted, and band-widths-at-half height ($\Delta\bar{\nu}_{0,1/2}$) decreased, due to an expected "rigid medium effect" in PEG-DMA550 film. The extent of loss of medium dipole reorientation in the rigid environment, and the increased emission energies in the film, resulted in enhanced emission quantum yields and excited state lifetimes in accordance with the energy gap law. The "rigid medium effect" in PEG-DMA550 is less pronounced than in films of poly(methyl methacrylate) (PMMA) pointing to a more fluid-like local environment presumably arising from the ethylene glycol linker spacers in PEG-DMA550. Comparison of the absorption, emission, emission spectral fitting, and emission lifetime results for $[Ru(dmb)_3](PF_6)_2$ and $[Ru(vbpy)_3](PF_6)_2$ shows that the vinyl groups of vbpy copolymerize with PEG-DMA550 covalently incorporating $Ru(vbpy)_3^{2+}$ as a cross-linker into the polymer network. The most dramatic effect of the fluid-to-film transition is seen in the emission lifetime data for $[Ru(phen)_3](p\text{-}Tos)_2$, with an increase of ∼3 in the PEG-DMA550 film. $Ru(phen)_3^{2+}$ cations appear to occupy a low symmetry site in the films probably close to the polar acrylate groups in a structurally confined environment.

Introduction

Given their charge transfer character, metal-to-ligand charge transfer (MLCT) transitions in polypyridyl complexes of $d\pi^6$ complexes of Ru(II), Os(II), and Re(I), both absorption and emission, have proven to be useful probes of medium effects.[1,2] In MLCT transitions, electrons are transferred from largely metal-based $d\pi$-orbitals to π^* orbitals on an acceptor ligand.[3] Significant insight into the response of the surrounding medium to excitation and excited state formation has been obtained by a combination of emission quantum yield, emission spectral fitting, and lifetime measurements in fluid media, glasses and frozen solutions, and in the glass-to-fluid transition.[4−6]

A complicating feature in MLCT photophysics arises from low-lying, metal-centered dd states of configuration $d\pi^5 d\sigma^{*1}$. These states are short-lived and provide an additional nonradiative decay pathway. Once occupied, they can lead to ligand-loss photochemistry.[7,8] Stabilization toward ligand loss has been achieved by modifying the MLCT-dd energy gap by ligand changes,[9−13] and encapsulating the complexes in rigid or film media such as poly(ethylene oxide),[14] zeolites,[15] sol−gel monoliths,[16−18] and poly(methyl methacrylate) (PMMA).[19] In rigid media, enhanced lifetimes are observed, in part, due to the enhanced MLCT-ground state energy gap induced by the rigidity of local medium dipoles and their inability to reorient to the new electronic configuration of the excited state.

In a recent study on $Ru(bpy)_3^{2+}$ and *cis*-$[Ru(bpy)_2(py)_2]^{2+}$ in PMMA, Thompson et al. noted that stabilization toward ligand loss in this rigid medium originated in an inhibition toward the large amplitude displacements associated with metal−ligand bond dissociation and not from an increased ^{3}MLCT-dd energy gap.[20] In fact, the ^{3}MLCT-dd energy gap is decreased relative to solution because of the sensitivity of the MLCT state to medium effects.

We have an interest in excited state properties and reactivity in rigid media both from a fundamental perspective and for possible device applications.[7,16,21] Recently, a new class of free-standing films was prepared by thermal[22,23] and/or photochemical[24,25] polymerization of vinyl-containing poly(ethylene glycol) dimethacrylate liquids (PEG-DMA), Figure 1. The polymerized PEG-DMA films, and the way they are prepared, offer distinct advantages. They are conformable to the shape of the container to the nanoscale and are accessible by thermal or photochemical initiation. Although related structurally to poly(methyl methacrylate), individual polymer strands are cross-linked because of the divinyl nature of the polymer precursor.[12] PEG-DMA films are formed solvent free with uniform thicknesses, with examples possessing varying degrees of hydrophilic character depending on the number of ethylene glycol spacers.

We describe here the results of a photophysical study on a series of Ru^{II}-polypyridyl-based MLCT excited states in PEG-DMA fluid solutions and in cross-linked films. The monomer precursor used (PEG-DMA550), Figure 1, contains nine repeating ethylene glycol spacers. It is ideal in forming optically transparent, conformable films that can be produced in any

* To whom corresondence should be addressed. E-mail: tjmeyer@email.unc.edu.

10.1021/jp107077t © 2011 American Chemical Society
Published on Web 12/14/2010

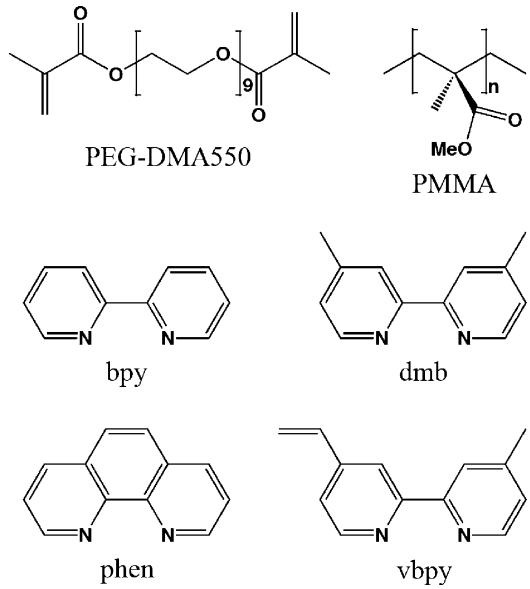

Figure 1. Structures of poly(ethylene glycol) dimethacrylate (PEG-DMA550) monomer, poly(methylmethacrylate) (PMMA), and the polypyridyl ligands.

geometry. The complexes chosen for study, $[Ru(bpy)_3](p\text{-}Tos)_2$, $[Ru(dmb)_3](PF_6)_2$, $[Ru(vbpy)_3](PF_6)_2$, and $[Ru(phen)_3](p\text{-}Tos)_2$ (bpy = 2,2′-bipyridine, dmb = 4,4′-dimethyl-2,2′-bipyridine, vbpy = 4-methyl-4′-vinyl-2,2′-bipyridine, phen = 1,10-phenanthroline, and *p*-Tos = *p*-toluene sulfonate), are representative of the broader class of well-defined polypyridyl Ru(II) MLCT excited states.[23]

The complexes were incorporated into the films by dissolving them in fluid PEG-DMA550 containing a diazo initiator followed by thermal polymerization. $[Ru(vbpy)_3](PF_6)_2$ was included as a member of the series to explore the use of the vinyl substituents on the polypyridyl ligands as a way to incorporate the chromophore into the growing polymer chain by covalent bond formation.

Experimental Section

Materials. $[Ru(dmb)_3](PF_6)_2$ and $[Ru(vbpy)_3](PF_6)_2$ were prepared by previously reported methods.[26,27] $[Ru(bpy)_3](p\text{-}Tos)_2$ and $[Ru(phen)_3](p\text{-}Tos)_2$ (*p*-Tos is *p*-toluene sulfonate) were precipitated from aqueous solutions of $[Ru(bpy)_3]Cl_2$ and $[Ru(phen)_3]Cl_2$ (Aldrich), respectively, by addition of 20 equiv of Na(*p*-Tos). Anhydrous acetonitrile was obtained from Burdick and Jackson and used without further purification. Poly(ethylene glycol) dimethacrylate (PEG-DMA550) liquid monomer was purchased from Aldrich. Purification of the PEG-DMA550 fluid and removal of the polymerization inhibitor (MEHQ) was achieved by passing the neat monomer through an alumina column. The cross-linking initiator (Vazo-52) was purchased from DuPont.

Sample Preparation. Samples were prepared by dissolving a complex salt in inhibitor-free liquid PEG-DMA550. Complex concentrations of $\sim 10^{-4}-10^{-5}$ M were used to achieve absorbances of 0.1−0.3 at $\lambda = 450$ nm. The solutions were placed in 1 cm path length glass cuvettes and freeze−pump−thaw degassed five times. For the polymerized samples, 1% by weight Vazo-52 was added to the chromophore/monomer solution with films formed by thermal curing under vacuum at 50 °C overnight to yield optically transparent, 1 cm thick samples.

Measurements

Absorbance and Steady-State Emission Spectra. UV−vis spectra in fluid and films were obtained by using a Varian Cary 50 UV−vis spectrophotometer. Steady-state emission spectra were acquired with a PTI 4SE-NIR QuantaMaster fluorimeter. Spectra were acquired on samples dissolved in thoroughly degassed PEG-DMA550 under optically dilute conditions (absorbance ∼0.1−0.3) and sealed under vacuum in 1 cm path length glass cuvettes. Radiative quantum yields (Φ_r) were determined relative to $[Ru(bpy)_3](PF_6)_2$ ($\Phi_r = 0.095$ in CH_3CN).[28] Quantum yields were calculated by using eq 1

$$\Phi_{unk} = \Phi_{std}\frac{(I_{unk}/A_{unk})}{(I_{std}/A_{std})}\left(\frac{\eta_{unk}}{\eta_{std}}\right)^2 \quad (1)$$

with Φ_{unk} and Φ_{std} the radiative quantum yields of sample and the standard, respectively. I_{unk} and I_{std} are the areas of emission profiles of sample and standard, and A_{unk} and A_{std} are the absorbances of the sample and standard at 450 nm. η_{unk} and η_{std} are the indices of refraction of sample and standard solutions (taken as the neat solvents).

Time-Resolved Emission Spectroscopy. Nanosecond time-resolved emission decays were obtained with a PTI GL-3000 pulsed nitrogen laser (337 nm, 6 Hz, 1 mJ) as input for a PTI GL-301 dye laser (440 nm, 6 Hz, 1 μJ) as an excitation source. Data were acquired at room temperature in thoroughly freeze−pump−thaw degassed fluid and solid PEG-DMA550 samples having absorbances between 0.1 and 0.3 at the excitation wavelength of 440 nm. Samples were sealed under vacuum in 1 cm path length glass cuvettes. A McPherson 272 monochromator and a Hamamatsu R-928 photomultiplier were used to detect emission at 90° relative to the excitation axis. Decay traces were constructed as an average of 500 transients monitored at the emission maximum for each compound. Decay traces were fit by using the SigmaPlot 11.0 software package.[29]

Emission Spectral Fitting. Emission spectra were fit by application of a one-mode Franck−Condon analysis given in eq 2[30,31]

$$I(\bar{\nu}) = \sum_{\nu_m=0}^{5}\left\{\left(\frac{E_0 - \nu_M\hbar\omega_M}{E_0}\right)^3\left(\frac{S_M^{\nu_M}}{\nu_M!}\right)\times \exp\left[-4\ln(2)\left(\frac{\bar{\nu} - E_0 + \nu_M\hbar\omega_M}{\Delta\bar{\nu}_{0,1/2}}\right)^2\right]\right\} \quad (2)$$

In eq 2, E_0 is the energy gap between the lowest energy ^{3}MLCT excited state and ground state, S_M is the electron-vibrational coupling constant or Huang−Rhys factor, $\hbar\omega_M$ is the quantum spacing for the medium frequency acceptor mode, and $\Delta\bar{\nu}_{0,1/2}$ is the width at half-maximum of the 0−0 vibronic component.

Spectral fitting was performed with a least-squares analysis program written by J. P. Claude.[32,33] Emission spectra were converted to units of quanta per second versus wavenumber following the procedure of Parker and Rees.[34] A global minimum of each fit was found by varying $\hbar\omega_M$, which was then fixed at 1350 cm^{-1} for all four complexes in both fluid and solid PEG-DMA550. The parameters E_0, S_M, and $\Delta\bar{\nu}_{0,1/2}$ were varied to find the global minimum at $\hbar\omega_M = 1350$ cm^{-1}.

Results

Absorption and Emission. Absorption and emission spectral data for the four complex salts $[Ru(bpy)_3](p\text{-}Tos)_2$,

TABLE 1: Photophysical Properties at Room Temperature in Fluid PEG-DMA550 (Top Entry) and Film PEG-DMA550 (Bottom Entry)

	λ_{Abs} (nm)[a]	λ_{Em} (nm)[b]	Φ_r	t_{obs} (ns)	k ($\times 10^6$ s^{-1})[c]	k_r ($\times 10^5$ s^{-1})[d]	k_{nr} ($\times 10^6$ s^{-1})[e]
[Ru(bpy)$_3$](*p*-Tos)$_2$	455	632	0.11	880	1.1 ± 0.05	1.2 ± 0.06	0.98 ± 0.05
	455	612	0.15	1350	0.74 ± 0.04	1.1 ± 0.06	0.63 ± 0.03
[Ru(dmb)$_3$](PF$_6$)$_2$	461	641	0.08	735	1.4 ± 0.1	1.1 ± 0.06	1.3 ± 0.1
	460	615	0.18	1215	0.82 ± 0.05	1.5 ± 0.1	0.67 ± 0.04
[Ru(vbpy)$_3$](PF$_6$)$_2$	470	655	0.11	1285	0.78 ± 0.04	0.86 ± 0.05	0.69 ± 0.03
	466	607	0.28	1720	0.58 ± 0.03	1.6 ± 0.1	0.42 ± 0.02
[Ru(phen)$_3$](*p*-Tos)$_2$	450	609	0.05	630	1.6 ± 0.1	0.80 ± 0.05	1.5 ± 0.1
	451	598	0.12	2000	0.50 ± 0.03	0.60 ± 0.03	0.44 ± 0.02
[Ru(bpy)$_3$](PF$_6$)$_2$[f]	454	616	0.095	985	1.02 ± 0.05	0.97 ± 0.05	0.92 ± 0.05
[Ru(bpy)$_3$](PF$_6$)$_2$[g]	454	590		1500	0.67		

[a] $^1A_1 \rightarrow {}^1$MLCT absorption maximum. [b] ^{3}MLCT $\rightarrow {}^1A_1$ emission maximum. [c] $k = \tau^{-1}$. [d] $k_r = \Phi_r k$. [e] $k_{nr} = k - k_r$. [f] Data in nitrogen purged CH_3CN. [g] PMMA film data from ref 20.

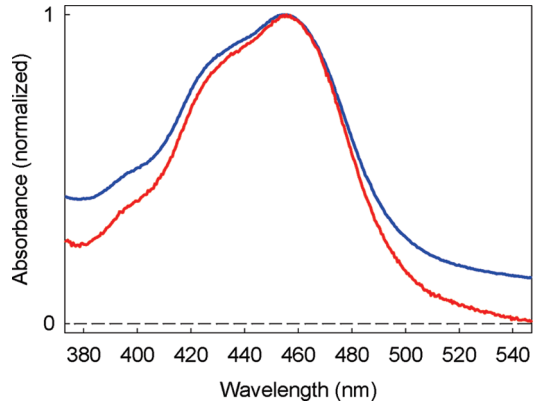

Figure 2. Near UV−vis absorption spectra for [Ru(bpy)$_3$](*p*-Tos)$_2$ in room-temperature PEG-DMA550 fluid (red trace) and film (blue trace).

[Ru(dmb)$_3$](PF$_6$)$_2$, [Ru(vbpy)$_3$](PF$_6$)$_2$, and [Ru(phen)$_3$](*p*-Tos)$_2$ (bpy = 2,2′-bipyridine, dmb = 4,4′-dimethyl-2,2′-bipyridine, vbpy = 4-methyl-4′-vinyl-2,2′-bipyridine, phen = 1,10-phenanthroline, and *p*-Tos = *p*-toluene sulfonate) in fluid and film PEG-DMA550 are summarized in Table 1. Spectra for [Ru(bpy)$_3$](*p*-Tos)$_2$ are shown in Figure 1 and for the others in Supporting Information Figures S1A−S1D. The higher energy, ligand-localized $\pi \rightarrow \pi^*$ transitions in the UV were not observable in the absorption spectra due to competitive absorption by the glass cuvettes. Visible absorption spectra are dominated by $^1A_1 \rightarrow {}^1$MLCT ($t_{2g} \rightarrow \pi^*$(NN), NN = polypyridyl ligand) transitions in the visible at ~450 nm, for example, similar to [Ru(bpy)$_3$](PF$_6$)$_2$ in CH_3CN.[35−37] Emission occurs from ^{3}MLCT $\rightarrow {}^1A_1$ transitions which have been extensively studied in both fluid and rigid media.[1,3,4,38]

Absorption band energies are nearly identical in fluid and film PEG-DMA550 suggesting similar local dielectric microenvironments in the two. Band shapes for emission from [Ru(bpy)$_3$](*p*-Tos)$_2$ in fluid and film at room temperature are similar, Figure 3, but with a blue shift of ~500 cm^{-1} in the film relative to the fluid.

Time-Resolved Emission. Excited-state lifetimes (τ_{obs}) for all four complexes, obtained by transient emission measurements in fluid and film PEG-DMA550, are reported in Table 1. Excited-state decays in both media are exponential except for [Ru(phen)$_3$](*p*-Tos)$_2$ in the polymerized film. For this complex, the slight heterogeneity in emission decay was fit to a stretched exponential function (Figures S2A−S2D).[39,40] Closely related results were obtained for the PF_6^- salt ruling out an anion effect. Lifetimes vary from 630 ns for [Ru(phen)$_3$](*p*-Tos)$_2$ in fluid PEG-DMA550 to an average lifetime of 2000 ns for [Ru(phen)$_3$](*p*-Tos)$_2$ in film PEG-DMA550. Emission decay traces for [Ru(bpy)$_3$](*p*-Tos)$_2$ in fluid and film PEG-DMA550 are shown in Figure 4 and, for comparison, [Ru(bpy)$_3$](PF$_6$)$_2$ in CH_3CN in the inset. Excited-state decay for [Ru(bpy)$_3$](*p*-Tos)$_2$ in PEG-DMA550 occurs with τ_{obs} = 1350 ns in the film and τ_{obs} = 880 ns in the fluid.

Emission Spectral Fitting. Emission spectral fitting parameters obtained from the single, average mode, Franck−Condon line shape analysis described in the Experimental Section are listed in Table 2. In the fits, the quantum spacing was fixed at 1350 cm^{-1}. The spectral fitting parameters were used to calculate vibrational overlap factors for nonradiative decay (ln[*F*(calc)]), eq 3.[30] Calculated values are listed in Table 2. Equation 3 is valid within the weak vibrational coupling ($E_0 \gg \hbar\omega_M$) and low-temperature limits ($\hbar\omega_M \gg k_bT$) and assumes the same quantum

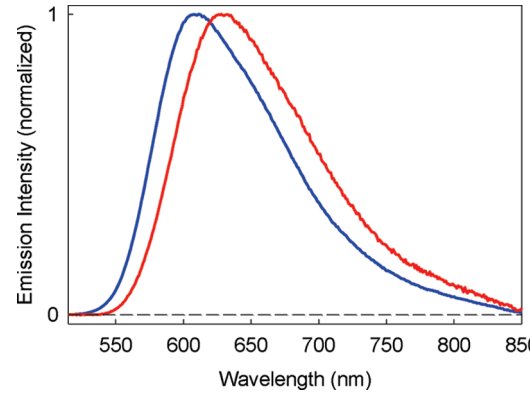

Figure 3. Steady-state emission spectra for [Ru(bpy)$_3$](*p*-Tos)$_2$ in room-temperature PEG-DMA550 fluid (red trace) and film (blue trace) (λ_{pump} = 450 nm).

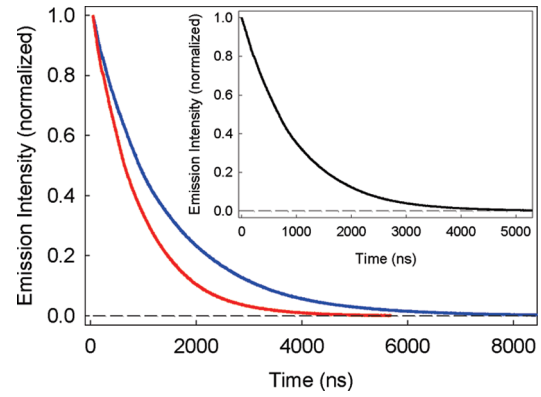

Figure 4. Nanosecond time-resolved emission decay for [Ru(bpy)$_3$](*p*-Tos)$_2$ in room-temperature PEG-DMA550 fluid (red trace) and film (blue trace) (λ_{pump} = 440 nm). Both decay traces were exponential with τ_{obs}^{film} = 1350 ns and τ_{obs}^{fluid} = 880 ns. The inset shows the decay trace for [Ru(bpy)$_3$](PF$_6$)$_2$ in nitrogen purged CH_3CN with τ_{obs}^{ACN} = 985 ns.

TABLE 2: Emission Spectral Fitting Parameters and Franck-Condon Factors in Fluid PEG-DMA550 (Top Entry) and Film PEG-DMA550 (Bottom Entry)

	E_0 (cm^{-1})	S_M	$\hbar\omega_M$ (cm^{-1})	fwhm (cm^{-1})	ln[F(calc)][a]
[Ru(bpy)$_3$](p-Tos)$_2$	16 060	0.91	1350	1830	−20.32
	16 550	0.94	1350	1685	−20.98
[Ru(dmb)$_3$](PF$_6$)$_2$	15 840	0.92	1350	1815	−19.80
	16 385	0.98	1350	1690	−20.22
[Ru(vbpy)$_3$](PF$_6$)$_2$	15 350	0.71	1350	1875	−21.43
	16 590	1.00	1350	1625	−20.41
[Ru(phen)$_3$](p-Tos)$_2$	16 540	0.81	1350	1740	−22.53
	16 890	0.87	1350	1700	−22.47
[Ru(bpy)$_3$](PF$_6$)$_2$[b]	16 320	1.10	1350	1750	−18.63
[Ru(bpy)$_3$](PF$_6$)$_2$[c]	16 950	1.14	1350	1500	−19.67

[a] Calculated from eq 3. [b] Parameters from data in CH_3CN solution. [c] PMMA film data taken from ref 20.

spacing for the initial and final states. S_M and $\hbar\omega_M$ are average values for contributions from series of symmetrical C=C and C=N stretching modes of the polypyridyl ligands.[30,41] Solvent and low-frequency modes are treated classically and included in $\Delta\bar{\nu}_{0,1/2}$.

$$\ln[F(\text{calc})] = -\frac{1}{2}\ln\left(\frac{\hbar\omega_M E_0}{(1000\ \text{cm}^{-1})^2}\right) - S_M - \frac{\gamma E_0}{\hbar\omega_M} + (\gamma+1)^2\left(\frac{\Delta\bar{\nu}_{0,1/2}}{\hbar\omega_M}\right)^2/16\ln 2 \quad (3)$$

$$\gamma = \ln\left(\frac{E_0}{S_M\hbar\omega_M}\right) - 1 \quad (4)$$

In the single average mode approximation, ln[F(calc)] is related to the nonradiative rate constant (k_{nr}) by eq 5

$$\ln(k_{nr}) = \ln(\beta_0) + \ln[F(\text{calc})] \quad (5)$$

In eq 5, β_0 includes the vibrationally induced electronic coupling matrix element that mixes the initial and final electronic states.

Discussion

As noted in the Introduction, the goal of this study was to explore the use of polymerizable fluids as media for photochemical and photophysical studies. The fluid−film combination chosen for study, PEG-DMA550, is one of a family of related dimethacrylates which differ in the number of ethylene glycol spacers between acrylate functional groups, Figure 1. Structurally, they are related to PMMA, which is also acrylate based, but without the intervening glycol spacers, Figure 1. They also differ from PMMA because of the dimethacrylate functional groups and cross-linking between polymer chains. PEG-DMA550 was chosen for initial study because of the superior optical properties of its cross-linked films.

Because of their well established photophysical properties and known medium dependence, the Ru(NN)$_3^{2+}$ (NN = polypyridyl ligand) MLCT excited states used in this study provided a direct probe into local environmental effects and the impact of the fluid-to-film transition on excited-state properties. Significant anion effects were also ruled out based on closely related results obtained for [Ru(dmb)$_3$](PF$_6$)$_2$ and [Ru(dmb)$_3$]Cl$_2$.

Photophysics of [Ru(bpy)$_3$](p-Tos)$_2$ and [Ru(dmb)$_3$](PF$_6$)$_2$: Case Studies in the Fluid-to-Film Transition in PEG-DMA550. Absorption maxima and band shapes for both [Ru(bpy)$_3$](p-Tos)$_2$ (Figure 2) and [Ru(dmb)$_3$](PF$_6$)$_2$ (Figure S1B) in fluid and film PEG-DMA550 are nearly superimposable, Table 1, showing that the optical dielectric properties of liquid and film are nearly the same. For these ground state D_3 complexes, in the limit of applicability of dielectric continuum theory and application of the dipole-in-a-sphere model, shifts in absorption energy (E_{abs}) between solvents are predicted to vary with the optical dielectric constant of the medium as in eq 6[1]

$$\Delta E_{abs} = \frac{\vec{\mu}_e^{\,2}}{a^3}\left(\frac{1 - D_{op}}{2D_{op} + 1}\right) \quad (6)$$

The similarities in emission band shapes for [Ru(bpy)$_3$](p-Tos)$_2$ (Figure 3) and [Ru(dmb)$_3$](PF$_6$)$_2$ (Figure S2B) in PEG-DMA550 film and fluid point to similar dielectric properties between the two media. Full-width at half-maximum values, $\Delta\bar{\nu}_{0,1/2}$, are lower in the films, and emission energies and 0−0 excited state energy gaps, E_0, are higher, Table 2. The increase in emission energies in the films has an impact on excited-state dynamics. For [Ru(bpy)$_3$](p-Tos)$_2$ (Figure 4) and [Ru(dmb)$_3$](PF$_6$)$_2$ (Figure S3B), τ_{obs}^{film} is ∼500 ns longer due to a combination of increased energy gaps (E_0) and Huang−Rhys factors (vibrational coupling constant, S_M) which decrease the vibrational overlap factor ln[F(calc)] calculated from eq 3.[26]

Differences in photophysical properties between fluid and rigid media are well documented for MLCT excited states.[42,43] Absorption is a vertical process in the Franck−Condon sense with intramolecular and medium modes frozen in configurations characteristic of the ground state on the time scale of the optical transition. Subsequent relaxation in these modes to configurations characteristic of the electronic configuration of the excited state leads to a decrease in excited-state energy and red-shifted emission. This includes the polarization field of the surrounding medium.

The transition between fluid and rigid media has been treated quantitatively by Marcus.[44,45] In the Marcus treatment, surrounding medium dipoles respond to the change in electronic configuration between excited and ground states from two sources, one frozen on the time scale of the excited state and one not. The frozen part arises from collective, large amplitude reorientations which are frozen in rigid media (λ_{oo}) and the nonfrozen part from single molecule rotations and phonon-like modes (λ_{oi}). The total solvent reorganizational energy (λ_o) in a rigid medium is given by eq 7

$$\lambda_o = \lambda_{oo} + \lambda_{oi} \quad (7)$$

In a rigid medium, λ_{oo} becomes part of the energy gap with $E_{o,fr} = E_{o,fl} + \lambda_{oo}$ (fr is frozen; fl is fluid) which is the origin of increased emission energies and energy gaps. The bandwidth at half-height ($\Delta\bar{\nu}_{0,1/2}$) is related to λ_o as in eq 8 with $\lambda_{o,fr} = \lambda_{o,fl} - \lambda_{oo,fl} = \lambda_{o,i}$.[1,46]

$$\lambda_{o,fr} = \lambda_{oi} = \frac{(\Delta\bar{\nu}_{0,1/2})^2}{16k_BT\ln 2} \quad (8)$$

A decrease in $\Delta\bar{\nu}_{0,1/2}$ in frozen media relative to the fluid is predicted, $(\Delta\bar{\nu}_{0,1/2})_{fl} - (\Delta\bar{\nu}_{0,1/2})_{fr} = 145\ cm^{-1}$ for $[Ru(bpy)_3](p\text{-}Tos)_2$ and 125 cm^{-1} for $[Ru(dmb)_3](PF_6)_2$. The increased energy gaps for $[Ru(bpy)_3](p\text{-}Tos)_2$ and $[Ru(dmb)_3](PF_6)_2$ in PEG-DMA550 film (Table 2) decrease vibronic overlap between the thermalized ^{3}MLCT excited state and $^1A_1$ ground state. The decrease in overlap decreases k_{nr} in the film as predicted by the energy gap law (eq 5).

From the $[Ru(bpy)_3](p\text{-}Tos)_2$ data in Table 1, $\ln(k_{nr}^{film})/\ln(k_{nr}^{fluid}) = 0.97$, and compared to the ratio of vibrational overlap factors of $\ln[F(calc,film)]/\ln[F(calc,fluid)] = 0.97$, suggesting that decay from the lowest MLCT state dominates k_{nr}.

Comparing Ru(bpy)$_3^{2+}$ Photophysics in PEG-DMA550 and PMMA Films. There are differences in emission maximum (Table 1), energy gap (E_0), and bandwidth at half-height ($\Delta\bar{\nu}_{0,1/2}$) for $[Ru(bpy)_3](p\text{-}Tos)_2$ in PEG-DMA550 and PMMA[20] (Table 2). They point to a difference in local microenvironments between the two polymer films. From Table 1, $\tau_{obs}^{PMMA} = 1500$ ns for $[Ru(bpy)_3](p\text{-}Tos)_2$ in PMMA compared to $\tau_{obs}^{film} = 1350$ ns in PEG-DMA550. These effects are anion independent with superimposable results for $[Ru(bpy)_3](p\text{-}Tos)_2$ and $[Ru(bpy)_3](PF_6)_2$ PEG-DMA550 fluid and film.

We have not attempted to model the rigidity differences between PMMA and PEG-DMA550 films quantitatively, but significant local structural differences between the two are expected. On the basis of the structures of the monomer precursors in Figure 1, PMMA forms a relatively tight, structurally rigid local environment. Even though PEG-DMA550 is a cross-linked polymer, there is more flexibility due to the extended ethylene glycol linkages between acrylates.

The difference between the two media appears in the photophysical properties. In comparing bandwidths $\Delta\bar{\nu}_{0,1/2}^{PMMA} = 1500\ cm^{-1}$ and $\Delta\bar{\nu}_{0,1/2}^{PEG550} = 1685\ cm^{-1}$ (Table 2), which from eq 8 gives $\lambda_{oi}^{PMMA} = 980\ cm^{-1}$ and $\lambda_{oi}^{PEG550} = 1235\ cm^{-1}$. The value for λ_{oi}^{PMMA} is consistent with 980 cm^{-1} calculated from the known static and optical dielectric constants of PMMA.[20] The increase in E_0 is predicted by the Marcus analysis with, $E_0^{PMMA} - E_0^{PEG550} = \lambda_{oo}^{PMMA} - \lambda_{oo}^{PEG550} = 400\ cm^{-1}$.

This analysis quantitates the difference between PEG-DMA550 and PMMA in their influence on MLCT excited-state properties. Given similarities in absorption band energies and shapes between the two, the local dielectric environments surrounding the complexes are similar, presumably dominated by the polar acrylate groups. However, in the more flexible environment around the complexes in PEG-DMA550, a more fluid-like relaxation occurs following excitation.

Even with the more flexible local environment, photochemical ligand loss in PEG-DMA550 is inhibited as found earlier in PMMA.[20] The evidence for this is the absence of Cl^- photosubstitution for dmb in $[Ru(dmb)_3]Cl_2$ in PEG-DMA550 even after the extensive photolysis periods used in conducting the lifetime measurements.

The decrease in excited-state energy of $\Delta E_0 = 400\ cm^{-1}$ for $Ru(bpy)_3^{2+*}$ in PEG-DMA550 compared with PMMA, Table 2, raises an additional point of interest for future study. In PMMA and other rigid or frozen media (low temperature glasses and solids) electron transfer is inhibited by two sources. One is an increase in free energy for electron transfer with λ_{oo} added to ΔG^o in frozen (fr) media relative to a comparable fluid (fl) with $\Delta G_{fr}^o = \Delta G_{fl}^o + \lambda_{oo}$[21,45] An additional reorganizational energy, λ_{X^-}, is added to ΔG^o from the frozen nature of the films removing the ability of counterions to respond to the change in local electric field associated with the electron transfer process. If sufficiently large in magnitude, these additional energy increments can increase ΔG^o to make electron transfer nonspontaneous. They also increase the classical barrier to electron transfer, $\Delta G^* = (\Delta G_{fl}^o + \lambda_{oo} + \lambda_{X^-} + \lambda_{oi})^2/4\lambda_{oi}$.[7,20] On the basis of this analysis, there may be significant differences in electron transfer rates and barriers between PMMA and PEG-DMA550.

Chromophore Incorporation into the Polymerized Acrylate Network: $[Ru(vbpy)_3](PF_6)_2$. For $Ru(vbpy)_3^{2+}$ in the salt $[Ru(vbpy)_3](PF_6)_2$, each polypyridyl ligand contains a polymerizable vinyl group ($-C(H)=CH_2$). Given the nature of the film forming polymerization process, this opens the possibility of incorporating the complex into the growing polymer film by chemical bond formation rather than as a solute trapped in the film structure.

In the film forming reactions, the concentration of complex, $\sim 10^{-5}$ M, was relatively low. Attempts to detect conversion of the $-(bpy)CH=CH_2$ vinyl groups in the complex into $-(bpy)CH-CH_2-$ linkers in the polymerized films by ^{1}H NMR and IR were unsuccessful. However, there is compelling evidence for vinyl incorporation from emission spectra (Figure S2C) and emission spectral fitting results for $[Ru(vbpy)_3](PF_6)_2$ in fluid and film PEG-DMA550 (Table 2) from the significantly lower E_0 and S_M values for fluid compared to film.

Electronic coupling of vinyl groups into the lowest π^*(vbpy) acceptor level delocalizes the excited electron onto the vinyl groups. This stabilizes the excited state decreasing the excited-to-ground state energy gap (E_0) and the extent of charge transfer. This decreases excited-to-ground state distortion in the acceptor ligand and S, the electron-vibrational coupling constant.[1,30]

By contrast, the CH_3 substituents in $Ru(dmb)_3^{2+}$ are electron donating relative to H, which increases the lowest π^*(dmb) level relative to bpy. This increases the energy gap and, with it, the extent of charge transfer resulting in increases in both E_0 and S_M. This difference between the initial vinyl groups as electron acceptors or donors, and how it is manifested in excited-state properties, provides a photophysical probe into covalent incorporation. From the data in Table 2, E_0 increases from 15 400 to 16 600 cm^{-1} in the film with the latter within experimental error of E_0 for $[Ru(dmb)_3](PF_6)_2$. S_M increases from 0.71 to 1.0. These changes also appear in the photophysical properties with a decrease in k_{nr} and corresponding increase in emission quantum yield.

The photophysical data are consistent with covalent incorporation. A schematic diagram of the covalently bound complex and its role as a cross-linker is shown in Figure 5.

Local Medium Effects for $[Ru(phen)_3](p\text{-}Tos)_2$. In contrast to the other complex salts, $[Ru(phen)_3](p\text{-}Tos)_2$ in PEG-DMA550 exhibits a significant increase in lifetime in the film compared to fluid, 630 to 2000 ns, Table 1. This is due to a decrease in k_{nr} by a factor of 3.4 even though the energy gap is only increased by 350 cm^{-1} and $\ln[F(calc)]$ is the same in the two media (Table 2). The origin of this effect is not clear. As noted above, nonradiative decay includes contributions from thermal activation and decay from an upper MLCT state and a low lying dd state or states. The contribution of the latter is greater in solution for $Ru(phen)_3^{2+*}$ than for $Ru(bpy)_3^{2+*}$, but a quantitative assessment of the possible role of a dd state or states in the films will require a detailed temperature dependent study.[20]

A notable result from the lifetime studies summarized in Table 1 is the 25% decrease in k_r in the film. The radiative rate constant is related to the Einstein coefficient for spontaneous emission (A) by eq 9.[30,47]

$$k_r = A = 8\pi\hbar cn^3\langle\bar{\nu}^{-3}\rangle^{-1}B \qquad (9)$$

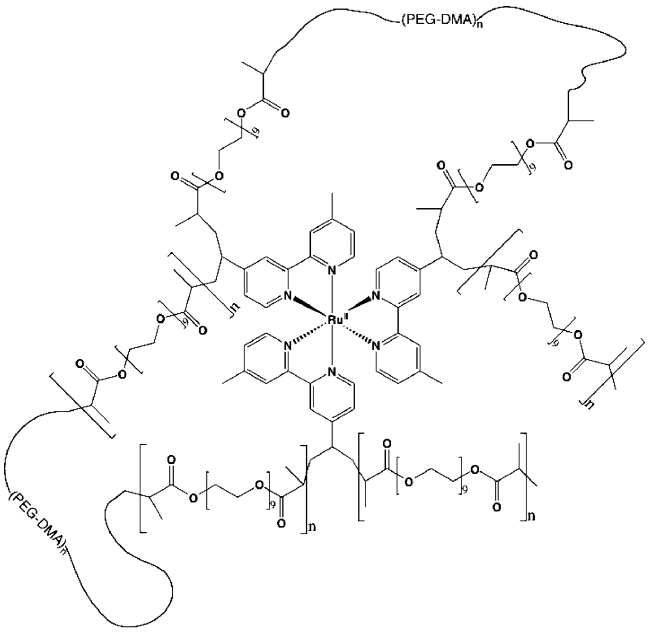

Figure 5. Illustration of the cross-linking covalent interaction proposed for $[Ru(vbpy)_3](PF_6)_2$ in PEG-DMA550 film resulting from copolymerization of the vinyl groups within the cross-linked network.

In eq 9, n is the refractive index of the medium and $\bar{\nu}$ the emission energy in cm^{-1}. The quantity $\langle \bar{\nu}^{-3} \rangle^{-1}$ is the inverse of the average value of $\bar{\nu}^{-3}$ ($\sim E_0^3$), and B is the transition probability for absorption. B is given by eq 10 with $\vec{M}$ the transition dipole moment.

$$B = \frac{8\pi^3}{3\hbar^2 c} |\vec{M}|^2 \tag{10}$$

Emission occurs from a manifold of three MLCT states from the lowest MLCT "triplet" with their degeneracy lifted by spin−orbit coupling. For $Ru(bpy)_3^{2+}$, the three low energy states are split by 100 cm^{-1} and behave as a single, thermally equilibrated state above 77 K.[48] The states differ in the extent of triplet character and in radiative lifetimes.[49−52] The transition dipole moment operator does not contain spin and dynamic interconversion between states, but relies on the extent of singlet mixing into the nominally triplet excited state(s). The ∼25% decrease in k_r in PEG-DMA550 film may be due to asymmetry in the local electronic environment which further splits the low energy manifold of states with emission dominated by a lowest state or states with a high degree of triplet character.

In any case, it is clear that, in contrast to the other complexes, $Ru(phen)_3^{2+}$ is a special case in responding significantly to the change from fluid to film PEG-DMA. The origin of the effect is not obvious. It is unlikely that the double bond linking the pyridyl halves of the ligand is involved in polymerization as for the vinyl groups in $Ru(vbpy)_3^{2+}$. MO calculations show that this bond does not contribute significantly to the lowest π^* acceptor level. It does impact nonradiative decay through increased rigidity and loss of torsional mode contributions to the decay process.[53]

Presumably the "$Ru(phen)_3^{2+}$ effect" is a local structural effect peculiar to this complex. In contrast to the fluid-like environment experienced by $Ru(bpy)_3^{2+}$ and the other complexes, $Ru(phen)_3^{2+}$ may be located in a relatively rigid region of the film close to polar acrylate groups in a structurally confined cavity.

Conclusions

As shown by a combination of absorption and emission spectra, emission spectral fitting, and lifetime measurements, PEG-DMA550 film prepared by thermal polymerization of the precursor fluid is a versatile medium for incorporating polypyridyl complex salts, $[Ru(bpy)_3](p\text{-}Tos)_2$, $[Ru(dmb)_3](PF_6)_2$, $[Ru(vbpy)_3](PF_6)_2$, and $[Ru(phen)_3](p\text{-}Tos)_2$, for spectroscopic and photophysical studies. The fluid-to-film transition has a characteristic impact on excited-state properties with increases in emission energies and quantum yields, increased 0−0 excited-to-ground state energy gaps, decreased band widths at half height ($\Delta\bar{\nu}_{0,1/2}$), and enhanced excited state lifetimes. This "rigid medium effect" is less pronounced than in films of poly(methyl methacrylate) (PMMA) pointing to a more fluid-like local environment presumably arising from the ethylene glycol linker spacers in PEG-DMA550. Emission spectral fitting comparisons for $[Ru(dmb)_3](PF_6)_2$ and $[Ru(vbpy)_3](PF_6)_2$ show that the vinyl groups of vbpy copolymerize with PEG-DMA550 covalently incorporating $Ru(vbpy)_3^{2+}$ into the polymer network by conversion of −(bpy)CH═CH_2 groups into −(bpy)CH−CH_2− linkers. Compared to the other complex salts, the MLCT lifetime of $[Ru(phen)_3](p\text{-}Tos)_2$ in PEG-DMA550 film is significantly enhanced, by a factor of ∼3, due to a combination of decreased nonradiative and radiative rates. In the film structure, $Ru(phen)_3^{2+}$ cations appear to occupy a relatively rigid, low symmetry environment near the polar acrylate groups of the film.

Acknowledgment. This work was supported by the Chemical Sciences, Geosciences, and Biosciences Division, Office of Basic Energy Sciences, U.S. Department of Energy under Grant DE-FG02-06ER15788. Salary support for A.P.G. was provided by the U.S. Department of Education under the Graduate Assistance in Areas of National Need (GAANN) program.

Supporting Information Available: Electronic absorption spectra (Figures S1A−S1D), steady-state emission spectra (Figures S2A−S2D), and time-resolved emission data (Figure S3A−S3D) for $[Ru(bpy)_3](p\text{-}Tos)_2$, $[Ru(dmb)_3](PF_6)_2$, $[Ru(vbpy)_3](PF_6)_2$, and $[Ru(phen)_3](p\text{-}Tos)_2$ in PEG-DMA550 fluid and film. This material is available free of charge via the Internet at http://pubs.acs.org.

References and Notes

(1) Chen, P. Y.; Meyer, T. J. *Chem. Rev.* **1998**, *98*, 1439.
(2) Yeh, A. T.; Shank, C. V.; McCusker, J. K. *Science* **2000**, *289*, 935.
(3) Campagna, S.; Puntoriero, F.; Nastasi, F.; Bergamini, G.; Balzani, V. *Photochemistry and Photophysics of Coordination Compounds I*; Springer-Verlag: Berlin, 2007; Vol. 280, p 117.
(4) Damrauer, N. H.; McCusker, J. K. *Inorg. Chem.* **1999**, *38*, 4268.
(5) Juris, A.; Balzani, V.; Barigelletti, F.; Campagna, S.; Belser, P.; von Zelewsky, A. *Coord. Chem. Rev.* **1988**, *84*, 85.
(6) Endicott, J. F.; Chen, Y. J. *Coord. Chem. Rev.* **2007**, *251*, 328.
(7) Fleming, C. N.; Dattelbaum, D. M.; Thompson, D. W.; Ershov, A. Y.; Meyer, T. J. *J. Am. Chem. Soc.* **2007**, *129*, 9622.
(8) Coe, B. J.; Friesen, D. A.; Thompson, D. W.; Meyer, T. J. *Inorg. Chem.* **1996**, *35*, 4575.
(9) Goze, C.; Chambron, J. C.; Heitz, V.; Pomeranc, D.; Salom-Roig, X. J.; Sauvage, J. P.; Morales, A. F.; Barigelletti, F. *Eur. J. Inorg. Chem.* **2003**, 3752.
(10) Barigelletti, F.; Decola, L.; Balzani, V.; Belser, P.; Vonzelewsky, A.; Vogtle, F.; Ebmeyer, F.; Grammenudi, S. *J. Am. Chem. Soc.* **1989**, *111*, 4662.
(11) Decola, L.; Barigelletti, F.; Balzani, V.; Belser, P.; Vonzelewsky, A.; Vogtle, F.; Ebmeyer, F.; Grammenudi, S. *J. Am. Chem. Soc.* **1988**, *110*, 7210.
(12) Barqawi, K. R.; Llobet, A.; Meyer, T. J. *J. Am. Chem. Soc.* **1988**, *110*, 7751.
(13) Treadway, J. A.; Loeb, B.; Lopez, R.; Anderson, P. A.; Keene, F. R.; Meyer, T. J. *Inorg. Chem.* **1996**, *35*, 2242.

(14) Campagna, S.; Bartolotta, A.; Dimarco, G. *Chem. Phys. Lett.* **1993**, *206*, 30.
(15) Kincaid, J. R. *Chem.—Eur. J.* **2000**, *6*, 4055.
(16) Adelt, M.; Devenney, M.; Meyer, T. J.; Thompson, D. W.; Treadway, J. A. *Inorg. Chem.* **1998**, *37*, 2616.
(17) Mongey, K.; Vos, J. G.; Maccraith, B. D.; McDonagh, C. M. *J. Sol-Gel Sci. Technol.* **1997**, *8*, 979.
(18) Glomm, W. R.; Volden, S.; Sjoblom, J.; Lindgren, M. *Chem. Mater.* **2005**, *17*, 5512.
(19) Fleming, C. N.; Jang, P.; Meyer, T. J.; Papanikolas, J. M. *J. Phys. Chem. B* **2004**, *108*, 2205.
(20) Thompson, D. W.; Fleming, C. N.; Myron, B. D.; Meyer, T. J. *J. Phys. Chem. B* **2007**, *111*, 6930.
(21) Jones, W. E.; Chen, P. Y.; Meyer, T. J. *J. Am. Chem. Soc.* **1992**, *114*, 387.
(22) Fleming, C. N.; Brennaman, M. K.; Papanikolas, J. M.; Meyer, T. J. *Dalton Trans.* **2009**, 3903.
(23) He, S. L.; Yaszemski, M. J.; Yasko, A. W.; Engel, P. S.; Mikos, A. G. *Biomaterials* **2000**, *21*, 2389.
(24) Hu, Z. K.; Chen, L.; Betts, D. E.; Pandya, A.; Hillmyer, M. A.; DeSimone, J. M. *J. Am. Chem. Soc.* **2008**, *130*, 14244.
(25) Kim, P.; Kim, D. H.; Kim, B.; Choi, S. K.; Lee, S. H.; Khademhosseini, A.; Langer, R.; Suh, K. Y. *Nanotechnology* **2005**, *16*, 2420.
(26) Damrauer, N. H.; Boussie, T. R.; Devenney, M.; McCusker, J. K. *J. Am. Chem. Soc.* **1997**, *119*, 8253.
(27) Devenney, M.; Worl, L. A.; Gould, S.; Guadalupe, A.; Sullivan, B. P.; Caspar, J. V.; Leasure, R. L.; Gardner, J. R.; Meyer, T. J. *J. Phys. Chem. A* **1997**, *101*, 4535.
(28) Ishida, H.; Tobita, S.; Hasegawa, Y.; Katoh, R.; Nozaki, K. *Coord. Chem. Rev.* **2010**, ASAP.
(29) *SigmaPlot ver 11.0*; Systat Software, Inc., 2008.
(30) Kober, E. M.; Caspar, J. V.; Lumpkin, R. S.; Meyer, T. J. *J. Phys. Chem.* **1986**, *90*, 3722.
(31) Kestell, J. D.; Williams, Z. L.; Stultz, L. K.; Claude, J. P. *J. Phys. Chem. A* **2002**, *106*, 5768.
(32) Claude, J. P. University of North Carolina at Chapel Hill, 1995.
(33) Claude, J. P.; Meyer, T. J. *J. Phys. Chem.* **1995**, *99*, 51.
(34) Parker, C. A.; Rees, W. T. *Analyst* **1960**, *85*, 587.
(35) Anderson, P. A.; Strouse, G. F.; Treadway, J. A.; Keene, F. R.; Meyer, T. J. *Inorg. Chem.* **1994**, *33*, 3863.
(36) Strouse, G. F.; Anderson, P. A.; Schoonover, J. R.; Meyer, T. J.; Keene, F. R. *Inorg. Chem.* **1992**, *31*, 3004.
(37) Kober, E. M.; Meyer, T. J. *Inorg. Chem.* **1982**, *21*, 3967.
(38) Barigelletti, F.; Belser, P.; Vonzelewsky, A.; Juris, A.; Balzani, V. *J. Phys. Chem.* **1985**, *89*, 3680.
(39) Williams, G.; Watts, D. C. *Trans. Faraday Soc.* **1970**, *66*, 80.
(40) Shlesinger, M. F.; Montroll, E. W. *Proc. Natl. Acad. Sci. U.S.A* **1984**, *81*, 1280.
(41) Caspar, J. V.; Westmoreland, T. D.; Allen, G. H.; Bradley, P. G.; Meyer, T. J.; Woodruff, W. H. *J. Am. Chem. Soc.* **1984**, *106*, 3492.
(42) Worl, L. A.; Meyer, T. J. *Chem. Phys. Lett.* **1988**, *143*, 541.
(43) Kitamura, N.; Kim, H. B.; Kawanishi, Y.; Obata, R.; Tazuke, S. *J. Phys. Chem.* **1986**, *90*, 1488.
(44) Marcus, R. A. *J. Phys. Chem.* **1990**, *94*, 4963.
(45) Chen, P. Y.; Meyer, T. J. *Inorg. Chem.* **1996**, *35*, 5520.
(46) Claude, J. P.; Omberg, K. M.; Williams, D. S.; Meyer, T. J. *J. Phys. Chem. A* **2002**, *106*, 7795.
(47) Strickler, S. J.; Berg, R. A. *J. Chem. Phys.* **1962**, *37*, 814.
(48) Crosby, G. A. *Acc. Chem. Res.* **1975**, *8*, 231.
(49) Yersin, H.; Humbs, W.; Strasser, J. *Coord. Chem. Rev.* **1997**, *159*, 325.
(50) Yersin, H.; Strasser, J. *Coord. Chem. Rev.* **2000**, *208*, 331.
(51) Lumpkin, R. S.; Kober, E. M.; Worl, L. A.; Murtaza, Z.; Meyer, T. J. *J. Phys. Chem.* **1990**, *94*, 239.
(52) Kober, E. M.; Meyer, T. J. *Inorg. Chem.* **1984**, *23*, 3877.
(53) Kober, E. M.; Meyer, T. J. *Inorg. Chem.* **1985**, *24*, 106.

JP107077T